ChemPubSoc Europe

DOI: 10.1002/open.201900043

ChemistryOPEN Communications

Commensurate $Nb_2Zr_5O_{15}$: Accessible Within the Field $Nb_2Zr_xO_{2x+5}$ After All

Dennis Wiedemann,*[a] Steven Orthmann,[a] Martin J. Mühlbauer,[b] and Martin Lerch[a]

Doped niobium zirconium oxides are applied in field-effect transistors and as special-purpose coatings. Whereas their material properties are sufficiently known, their crystal structures remain widely uncharacterized. Herein, we report on the comparably mild sol-gel synthesis of $Nb_2Zr_5O_{15}$ and the elucidation of its commensurately modulated structure via neutron diffraction. We describe the structure using the most appropriate superspace as well as the convenient supercell approach. It is part of an α-PbO_2-homeotypic field with the formula $Nb_2Zr_xO_{2x+5}$, which has previously been reported only for $x \geq 5.1$, and is closely related to the structure of $Hf_3Ta_2O_{11}$. The results, supported by X-ray diffraction and additional synthesis experiments, are contextualized within the existing literature. Via the sol-gel route, metastable Nb–Zr–O compounds and their heavier congeners are accessible that shed light on possible structures of these commercially utilized materials.

Doped niobium zirconium oxides are regularly used in metal-oxide-semiconductor field-effect transistors (MOSFETs) and as coatings for special applications – without proper characterization of their crystal structures.[1] Their first representatives with formulae between $Nb_2Zr_4O_{13}$ and Nb_8ZrO_{22} were reported as solid solutions with the structure of cubic zirconia in 1952.[2] A few years later, Roth and Coughanour published a first *x*–*T* phase diagram of $Nb_{2x}Zr_{1-x}O_{2+3x}$ ($0 \leq x \leq 1$) showing the then hypothetic "$Nb_2Zr_5O_{15}$" as a $Nb_2Zr_6O_{17}$-like solid solution.[3] The existence and orthorhombic unit cell of the latter – typical for the whole range – were confirmed afterwards.[4] Additionally, Roth et al. found a sequence of non-overlapping $Nb_2Zr_nO_{2n+5}$ regions ($5 \leq n \leq 8$), which can be described as α-PbO_2-homeotypic superstructures of this unit cell.[5] Because of the imprecision of elemental analyses, however, the fringes remained fuzzy: A distinction between the candidates $Nb_2Zr_5O_{15}$ and $Nb_2Zr_{4.5}O_{14}$ for a sevenfold supercell was not possible. With the advent of the correspondent terminology in the 1990s, Thompson et al. presented a continuous field of incommensurately modulated structures for $Nb_2Zr_xO_{2x+5}$ ($5.1 \leq x \leq 8.3$) and explicitly – and soundly – excluded $Nb_2Zr_5O_{15}$ in favor of a mixture of $Nb_2Zr_{5.1}O_{15.2}$ and $Nb_{24}ZrO_{62}$.[6] Furthermore, they brought up problems reproducing the solid-state syntheses of past authors with respect to the accuracy of cation ratios. Other, more material-oriented groups described powders with compositions between $Nb_2Zr_7O_{19}$ and $Nb_2Zr_4O_{13}$ as single phases.[7] After 2000, scholarly literature mentions $Nb_2Zr_5O_{15}$ only once, namely as a single phase showing ordinary thermal expansion, without addressing its structure.[8] Overall, niobium zirconium oxides and their heavier tantalum and/or hafnium congeners are described as isotypic; solid-state synthesis using temperatures above 1300 °C is usual.

Herein, we report on the sol-gel synthesis of $Nb_2Zr_5O_{15}$, a compound at the niobium(V)-rich side of the field of α-PbO_2 homeotypes, and the elucidation of its commensurately modulated structure via neutron diffraction (ND). We describe it in modern terms using the superspace as well as the supercell approach and comment on the accessibility of the compound.

Initial powder X-ray diffraction (XRD), which we carried out on a sample synthesized with a molar Nb/Zr ratio of 1:2, only showed reflections consistent with a single phase of the α-PbO_2 type, even after long measuring time. As this is incompatible with the envisaged composition "$Nb_{0.33}Zr_{0.67}O_{2.17}$" (i.e., "$Nb_2Zr_4O_{13}$"), we performed ND, which is capable of revealing oxide ions even in the presence of ions as heavy as niobium(V) and zirconium(IV). To our surprise, many more reflections than in the X-ray diffractogram were visible, hinting at a modulated structure or multi-phase system. The recent structure elucidation of the closely related $Hf_3Ta_2O_{11}$, which we had achieved using electron tomography,[9] enabled us to adapt a $Nb_2Zr_5O_{15}$ model for Rietveld refinement against the ND data.

For the sake of consistency, we stuck to the absence-derived superspace-group setting *Xmcm*(00γ)*s*00 with the supercentering vector ($^1/_2$ $^1/_2$ 0 $^1/_2$) instead of the standard *Cmcm*(10γ)*s*00 or the equivalent setting *Amma*(α10)0*s*0 used in earlier literature. During refinement in superspace, a strong anisotropic (i.e., *hklm*-dependent) reflection broadening became obvious that is invisible in XRD and thus attributed to the oxide substructure. Use of an adequate strain-like model showed that mainly satellite reflections are affected ($M = 2$; see Table S1 in Supporting Information). This means that variations of the modulation vector ***q*** play a large role compared to only minor variations of

[a] Dr. D. Wiedemann, Dr. S. Orthmann, Prof. Dr. M. Lerch
Institut für Chemie
Technische Universität Berlin
Straße des 17. Juni 135, 10623 Berlin (Germany)
E-mail: dennis.wiedemann@chem.tu-berlin.de
[b] Dr. M. J. Mühlbauer
Heinz Maier-Leibnitz Zentrum (MLZ)
Technische Universität München
Lichtenbergstraße 1, 85747 Garching (Germany)

Supporting information for this article is available on the WWW under https://doi.org/10.1002/open.201900043

Table 1. Crystallographic Data for $Nb_2Zr_5O_{15}$ Powder.

	Superspace Model	Supercell Model
Sum formula	$Nb_{0.571}Zr_{1.429}O_{4.286}$	$Nb_2Zr_5O_{15}$
Crystal system	orthorhombic	orthorhombic
Space group	$Xmcm(00\gamma)s00$	$Pbnm$
a/Å	4.93881(11)	4.93881(11)
b/Å	5.29821(12)	5.29821(12)
c/Å	5.14909(13)	36.0436(9)
$\boldsymbol{q}$	$^1/_7\boldsymbol{c}^*$	–
V/Å^{-3}	134.735(5)	943.15(4)
Z	2	4
ρ_{calcd}/g cm^{-3}	6.2109	6.2109
$2\theta_{max}$	151.90	151.90
Measured/observed[a] reflections	708/686	708/686
Main reflections	156/152	–
First-order satellites	275/263	–
Second-order satellites	277/271	–
Data/parameters	2838/55	–[b]
R_p, wR_p[c]	0.0158, 0.0195	–[b]
R_{exp}, S	0.0119, 1.64	–[b]
R_F, wR_F[b]	0.0082, 0.0115	–[b]
R_B, wR_B[b]	0.0136, 0.0228	–[b]
$\Delta\rho_b$(min, max)/fm Å^{-3}	−0.14, 0.14	–[b]

[a] $I > 3\sigma(I)$. [b] Structure not refined in supercell description (see text). [c] $w = 1/[\sigma^2(I) + (0.01I)^2]$.

the average-lattice parameters a, b, and c.[10] Incomplete supercells at crystallite boundaries in the supposedly nanocrystalline powder may cause $\boldsymbol{q}$ to locally adapt, or stable incommensurately modulated compounds from the close $Nb_2Zr_xO_{2x+5}$ field may be admixed. Because of this, care was taken not to impose undue restrictions on $\boldsymbol{q}$. When the final stages of refinement with isotropic displacement parameters resulted in a value of $\boldsymbol{q} = 0.14281(14)\boldsymbol{c}^*$, however, we fixed it at $^1/_7 = 0.\overline{142857}$ and applied program routines for commensurate modulation. Refinement indicators (see Table 1) and the fitting of observed and calculated diffractograms (see Figure 1) suggest that the final model is well supported by the data. The soundness of modulation parameters was assured by inspecting de-Wolff sections (cf. Figure S2–S5 in Supporting Information).

Whereas satellite reflections dominate the neutron diffractogram, they are way less outstanding in XRD, because the modulation predominantly manifests in the anion substructure. Overall and selective broadening further diminish their maximum intensities, so that mainly the range $32° \leq 2\theta \leq 47°$ is left for visual discrimination of modulated and non-modulated structures (see Figure S6–S7 in Supporting Information). Refinement against X-ray data is viable but generally of low stability. Despite long measurements yielding high signal-to-noise ratios, it is impossible to refine atomic modulation parameters or even $|\boldsymbol{q}|$. An α-PbO_2-type model, however, fits considerably worse than the ND-derived modulated one (see Figure S7 in Supporting Information).

For refinement, we stuck to the (3+1)D superspace approach because it allows appropriate modelling with a restricted number of atomic parameters. For structure description, however, we provide an equivalent 1×1×7 supercell model that is easier to comprehend and compatible with most crystallographic software. From the one cation ($M1$) and three oxide positions (O1, O2, O3) in superspace, four cation ($M11$–$M14$) and eight oxide positions (O11–O14, O21–O23, O31) are generated in the supercell. The resulting structure is closely related to that of $Hf_3Ta_2O_{13}$,[9] differing from it primarily in the length of the modulation vector ($^1/_7\boldsymbol{c}^*$ instead of $^1/_5\boldsymbol{c}^*$) and thus in the sequence of cation coordination polyhedra. In $Nb_2Zr_5O_{15}$, distorted octahedra (coordination number [CN]: 6; green in Figure 2), capped trigonal prisms (CN: 7, two unique instances; turquoise), and distorted bicapped trigonal prisms (CN: 8; blue) form slabs that are stacked along c. The septempartite motive 6-7-7-8-7-7-6 repeats once per supercell. Two additional contacts (dashed lines in Figure 2) are present that would augment some polyhedra to capped octahedra (CN: 6+1, $d[M11\cdots O21] = 2.705[2]$ Å) and bicapped trigonal prisms (CN: 7+1, $d[M11\cdots O31] = 2.509[4]$ Å). Because of their distinct lengths, however, we do not consider them bonding. The largest deviation of the XRD-derived from the ND-derived model is in the average position of O3 (i.e., the position of O31 in the supercell model; yellow in Figure 2), leading to a larger contact distance of $d(M11\cdots O31) = 2.841(13)$ Å therein.

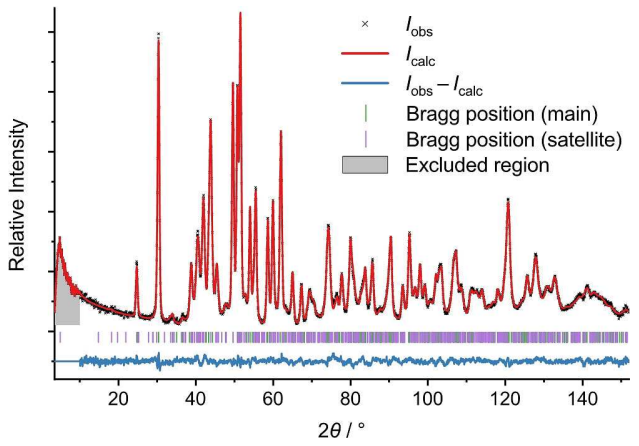

Figure 1. Neutron diffractogram ($\lambda = 1.54829$ Å) of $Nb_2Zr_5O_{15}$ at ambient temperature.

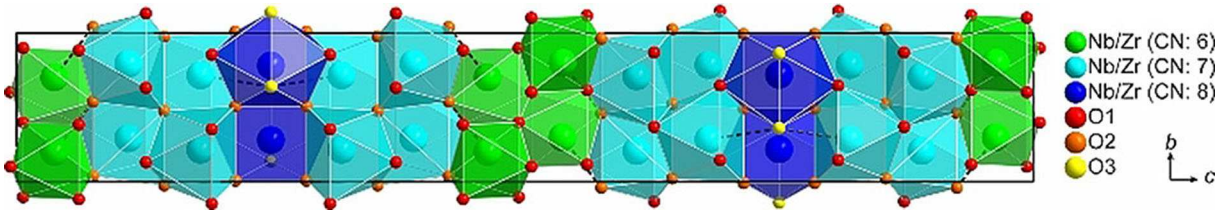

Figure 2. Crystal structure of $Nb_2Zr_5O_{15}$ (supercell model). Atoms with arbitrary radii, non-bonding contacts as grey dashed lines, unit cell in black.

Table 2. BVS, Mismatches, and Derived Relative Cation Occupations.

	CN	BVS	Mismatch	Relative Occupations
$Nb^{V}11/Zr^{IV}11$	6	3.897/4.080	−1.103/0.080	7:93
$Nb^{V}12/Zr^{IV}12$	7	3.760/3.935	−1.240/−0.065	0:100[a]
$Nb^{V}13/Zr^{IV}13$	7	3.921/4.107	−1.079/0.107	9:91
$Nb^{V}14/Zr^{IV}14$	8	4.226/4.424	−0.774/0.424	35:65

[a] Negative mismatches for both ions led to a physically meaningless negative occupation for $Nb^{V}12$.

Table 3. Cell Dimensions According to Le-Bail Fits on X-Ray Diffraction Data.

	"$Nb_2Zr_3O_{11}$"	$Hf_5Ta_2O_{15}$
Crystal system	orthorhombic	
Space group	$Xmcm(00\gamma)s00$	
a/Å	4.92566(16)	4.9690(7)
b/Å	5.31338(16)	5.2874(7)
c/Å	5.17325(16)	5.1394(6)
q/c^*[a]	0.1787(3)	0.1674(12)
V/Å^{-3}	135.394(9)	135.03(4)
R_p, wR_p[b]	0.0124, 0.0169	0.0222, 0.0355
S	2.11	3.80

[a] Raw estimates based on the very weak first-order satellite reflections. [b] $w = 1/[\sigma^2(I) + (0.01I)^2]$.

The different coordination environments suggest that the cations may be ordered on their preferred positions. Unfortunately, zirconium(IV) and niobium(V) ions cannot be distinguished via either X-ray or neutron diffraction, because they are isoelectronic and their coherent scattering lengths differ by merely ca. 1.5%. Bond-valence sums (BVS) and their mismatches with the ideal metal valences (oxidation numbers) are of little use to solve this problem (see Table 2). All positions are strongly underbonded for niobium(V), with Nb14 being the least disfavored. The metal(V) BVS are noticeably lower than in $Hf_3Ta_2O_{13}$,[9] which is probably caused by the higher relative number and thereby stronger predominance of metal(IV) ions. With a calculated overall ratio of $r(Nb/Zr) = 2:19$, the BVS cannot account for a clear separation of cations and leaves a scenario with Nb11/Zr11, Zr12, Nb13/Zr13, and Nb14 as most probable candidate.

In spite of providing niobium and zirconium in a molar ratio of 1:2 for synthesis, diffraction showed $Nb_2Zr_5O_{15}$ as the only crystalline product. We assume that the sample contains amorphous Nb_2O_5 as a second phase. Whereas the measured oxygen content is compatible with ratios of both 1:2 ($w_{calcd} =$ 27.41%) and 2:5 ($w_{calcd} = 27.21$%), gas pycnometry yields a value less than the crystallographic mass density of $Nb_2Zr_5O_{15}$ alone. This complies with an admixture of Nb_2O_5, which has a considerably lower density reported as 4.36–4.55 g cm^{-3}.[11]

Almost all reported synthesis routes for the compounds $Nb_2Zr_xO_{2x+5}$ employ a solid-state approach: The metal oxides are mixed, pressed into pellets, and heated to 1300–1600 °C in platinum tubes or foil. (With one brief mention each, the co-precipitation of hydroxides followed by condensation[4] and the oxygenation of a metal alloy[5] constitute exceptions.) Some of the protocols are known to suffer from niobium loss to the reaction vessels.[6a] We, on the other hand, have chosen a comparably mild sol-gel route employing alumina crucibles, for which such a niobium loss would be unprecedented. To solve the remaining questions about synthesis conditions, we had to rely on XRD as analytical method, which shows diagnostically useful and visually discernible reflections in the range of $32° \leq 2\theta \leq 47°$.

- An excess of the metal(V) compound (as applied for the ND samples) is not necessary for the sol-gel synthesis of $Nb_2Zr_5O_{15}$ or $Hf_3Ta_2O_{11}$ (see Figure S8–S9 in Supporting Information).
- Synthesis experiments aiming at the homologues $Hf_5Ta_2O_{15}$ and $Nb_2Zr_3O_{11}$ have been indecisive. Indeed, the products seem to belong to the field of modulated α-PbO_2-homeotypic compounds. The diffractogram of $Hf_5Ta_2O_{15}$ is compatible with an $Nb_2Zr_5O_{15}$-isotypic structure but suffers from further reflection broadening due to low crystallinity. The diffractogram of "$Nb_2Zr_3O_{11}$", on the other hand, exhibits additional small reflections hinting at the existence of multiple phases (see Figure S10–S11 in Supporting Information). Le-Bail fits allowed extraction of cell parameters (see Table 3) that should, however, be assessed with the advised caution.[12] Especially, trials of fixing $|\boldsymbol{q}|$ at different sensible values yielded results of similar quality. Rietveld refinements of atomic models against XRD data alone are unwarranted.
- The accessibility of these compounds depends on the choice of synthesis conditions. In our hands, a classical solid-state route (1500 °C) led to a mixture of a α-PbO_2-homeotypic compound, baddeleyite-type ZrO_2, and an unknown minor phase instead of single-phase $Hf_3Ta_2O_{11}$ (see Figure S12 in Supporting Information). Therefore, we deem $Nb_2Zr_5O_{15}$ and $Hf_3Ta_2O_{11}$ metastable.

With $Nb_2Zr_5O_{15}$ now and $Hf_3Ta_2O_{11}$ before,[9] we have synthesized two compounds off stoichiometry via a sol-gel route that "locked in" to commensurately modulated structures $M^{IV}{}_nM^{V}{}_2O_{2n+5}$ (M: metals) with the next higher metal(IV) content. An excess of metal(V) precursors is unnecessary for synthesis. Before, Thompson et al. have found a "lack of any evidence for [the length of the modulation vector] 'locking in' to a rational fraction" after solid-state synthesis at $\vartheta \geq 1300$ °C.[6a] They have also determined $x = 5.1$ as the lower stability limit of the $Nb_2Zr_xO_{2x+5}$ field. We attribute these results to the fact that $Nb_2Zr_5O_{15}$ and $Hf_3Ta_2O_{11}$ are metastable and only accessible via synthesis at lower temperatures. In spite of their crystal-chemical similarity, a homology between Zr–Nb and Hf–Ta compounds does not hold strictly in the cases at hand. In light of their technological application, these results bring us one step closer to a sound structural understanding of the compounds $(Nb,Ta)_2(Zr,Hf)_xO_{2x+5}$ that could be furthered with a systematic neutron/electron diffraction study over the whole (meta)stability range.

Experimental Section

Ternary compounds were synthesized from solutions of hafnium, niobium, tantalum, and zirconium citrates via a modified Pechini sol-gel route at 800 °C.[13] For the ND sample of $Nb_2Zr_5O_{15}$, an excess of niobium citrate ($r = 1:2$) was applied. Elemental analysis calcd (%) for $Nb_2Zr_5O_{15}$: O 27.21; found: O 27.26(8); ρ_{measd} (gas pycnometry): 5.98(9) g cm^{-3}. For comparison, the synthesis of $Nb_2Zr_5O_{15}$ was also tried via a solid-state route at 1500 °C starting from Nb_2O_5 and ZrO_2.

Powder XRD was carried out at ambient temperature on a "PANalytical X'Pert PRO MPD" diffractometer equipped with a "PIXcel" detector using nickel-filtered Cu-K_α radiation. Additional investigations were performed on a "Rigaku SmartLab 3 kW" system equipped with a Johansson-type Ge monochromator using Cu-$K_{\alpha1}$ radiation. Powder ND was carried out at ambient temperature with the high-resolution powder diffractometer SPODI at Heinz Maier-Leibnitz Zentrum (MLZ) in its standard setting ($\lambda = 1.54829$ Å).[14] Le-Bail fits, Rietveld refinement of an adjusted (3 + 1)D-superspace model derived from $Hf_3Ta_2O_{11}$,[9] and all following calculations were performed using JANA2006.[15] Bond-valence sums were calculated using VaList.[16]

For extensive experimental details, see section 1 of the Supporting Information. CCDC 1893626 and 1893627 contain the supplementary crystallographic data for this paper. These data can be obtained free of charge from The Cambridge Crystallographic Data Centre via www.ccdc.cam.ac.uk/structures.

Acknowledgements

This work is in part based upon experiments performed at the SPODI instrument operated by FRM II at the Heinz Maier-Leibnitz Zentrum (MLZ), Garching, Germany. Financial support by the Deutsche Forschungsgemeinschaft (SPP 1613, LE 781/13-2) is gratefully acknowledged. The authors thank Dr. Stefan Berendts (TU Berlin) for conducting oxygen analysis. The TOC graphic is a derivative work of "Electronic component – various unipolar power transistors"[17] by FDominec, used under CC BY-SA 3.0.[18]

Conflict of Interest

The authors declare no conflict of interest.

Keywords: neutron diffraction · niobium · sol-gel processes · X-ray diffraction · zirconium

[1] T. H. Baum, C. Xu, W. Paw, B. C. Hendrix, J. F. Roeder, Z. Wang (Advanced Technology Materials, Inc.), USA 20020132048, **2002**.
[2] a) E. A. Durbin, C. G. Harman (Battelle Memorial Institute), *U. S. A. E. C.* **1952**, *BMI-791*, 1–12; b) E. A. Durbin, H. E. Wagner, C. G. Harman (Battelle Memorial Institute), *U. S. A. E. C.* **1952**, *BMI-792*, 1–15.
[3] R. S. Roth, L. W. Coughanour, *J. Res. Natl. Bur. Stand. (U. S.)* **1955**, *55*, 209–213.
[4] V. K. Trunov, Z. A. Vladimirova, L. M. Kovba, L. N. Komissarova, *Izv. Akad. Nauk SSSR Neorg. Mater.* **1965**, *1*, 1152–1154.
[5] R. S. Roth, J. L. Waring, W. S. Brower, H. S. Parker, *NBS Spec. Publ. (U. S.)* **1972**, *364*, 183–195.
[6] a) J. G. Thompson, R. L. Withers, J. Sellar, P. J. Barlow, B. G. Hyde, *J. Solid State Chem.* **1990**, *88*, 465–475; b) R. L. Withers, J. G. Thompson, B. G. Hyde, *Acta Crystallogr. Sect. B* **1991**, *47*, 166–174.
[7] a) G. Gritzner, C. Puchner, *J. Eur. Ceram. Soc.* **1994**, *13*, 387–394; b) A. Pissenberger, G. Gritzner, *J. Mater. Sci. Lett.* **1995**, *14*, 1580–1582.
[8] M. J. Dejneka, C. L. Chapman, S. T. Misture, *J. Am. Ceram. Soc.* **2011**, *94*, 2249–2261.
[9] D. Wiedemann, T. Lüdtke, L. Palatinus, E. Willinger, M. G. Willinger, M. J. Mühlbauer, M. Lerch, *Inorg. Chem.* **2018**, *57*, 14435–14442.
[10] A. Leineweber, V. Petříček, *J. Appl. Crystallogr.* **2007**, *40*, 1027–1034.
[11] a) A. Vaskevich, M. Rosenblum, E. Gileadi, *J. Electrochem. Soc.* **1995**, *142*, 1501–1508; b) D. Rama Devi, G. Kalyani, K. S. Sastry, *J. Electrochem. Soc. India* **1989**, *38*, 291–292; c) J. Li, J.-j. Wen, H.-y. Zhong, D.-q. Yi, *Rare Met. Cem. Carbides* **2005**, *33*, 4–8.
[12] V. K. Peterson, *Powder Diffr.* **2005**, *20*, 14–17.
[13] M. P. Pechini (Sprague Electric Company), USA 3330697, **1967**.
[14] M. Hoelzel, A. Senyshyn, O. Dolotko, *J. Large-Scale Res. Facil.* **2015**, *1*, A5.
[15] V. Petříček, M. Dušek, L. Palatinus, *Z. Kristallogr. – Cryst. Mater.* **2014**, *229*, 345–352.
[16] A. S. Wills, VaList, Bond Valence Calculations and Listing, University College London, London, UK, **2011**.
[17] F. Dominec, "Electronic component - various unipolar power transistors", to be found under https://commons.wikimedia.org/wiki/File:Electronic_component_mosfets.jpg.
[18] CreativeCommons, "Attribution-ShareAlike 3.0 Unported – CC BY-SA3.0", to be found under https://creativecommons.org/licenses/by-sa/3.0/.

Manuscript received: January 28, 2019
Accepted: February 26, 2019